



Cite this: *RSC Adv.*, 2025, **15**, 50531

Received 8th December 2025  
Accepted 9th December 2025

DOI: 10.1039/d5ra09492e

rsc.li/rsc-advances

## A binuclear thorium complex with a Th–O–Th unit

Yifei He,<sup>†ab</sup> Yichen Huang,<sup>†c</sup> Kang Liu,<sup>†d</sup> Congzhi Wang,<sup>b</sup> Xiangyu Liu,<sup>id</sup> <sup>\*a</sup>  
Liyong Yuan,<sup>id</sup> <sup>b</sup> Jipan Yu,<sup>\*,b</sup> Yan Guo,<sup>id</sup> <sup>\*ab</sup> and Weiqun Shi,<sup>id</sup> <sup>\*bc</sup>

Complex **1**,  $[(\text{Trapen}^{\text{TMS}}\text{Th}\text{Cl}]$ ,  $\text{Trapen}^{\text{TMS}} = \text{N}(\text{CH}_2\text{Ph}(o\text{-NSiMe}_3)_3)$ , reacts with sodium azide to afford the dimeric complex **2**,  $[(\text{Trapen}^{\text{TMS}}\text{N}_3\text{Th})_2]$ . Treatment of **2** with  $\text{KC}_8$  yields a binuclear oxo-bridged thorium complex **3**,  $[(\text{Trapen}^{\text{TMS}}\text{Th})_2(\mu\text{-O})]$ . The crystal structure of **3** reveals a highly symmetrical configuration with a Th–O–Th unit, and the Th–O bond length is  $2.271(2)$  Å. Density functional theory calculations indicate significant covalent character in the Th–O–Th interaction, surpassing that in related Th–N–Th systems and the Th–O bonding in complex **3** displays stronger covalent interactions.

## 1 Introduction

Over the past decade, due to their unique electronic configurations and structural adaptability, actinide chemistry has attracted significant interest.<sup>1–6</sup> This is attributed to their large ionic radii and variable coordination geometries.<sup>7–15</sup> Among these, uranium and thorium occupy a privileged position in actinide research because they are accessible in standard laboratory settings, while transuranic elements require specialized containment infrastructure.<sup>16–18</sup> Recently, there has been burgeoning interest in the bonding modes between uranium-ligand and uranium-metal,<sup>17–26</sup> which stems from the desire to gain a deeper understanding of the chemical bonding of uranium and to establish a connection between it and observed physicochemical properties.<sup>24,27–29</sup>

Despite the numerous significant and increasing research findings regarding the chemical bonds of U–C/N/O in recent years,<sup>19,22,28,30–32</sup> An–X–An complexes have been rarely reported especially the Th–X–Th species. Compared with uranium (whose chemical bonding paradigms involves partial 5f orbital hybridization), the Th(IV) ion exhibits negligible 5f orbital participation in bonding. This is due to its larger ionic radius (94 pm for Th(IV) vs. 89 pm for U(IV)) and diminished radial extension of the 5f orbitals.<sup>33</sup> This difference confines the bonding of thorium predominantly due to electrostatic interactions, rendering thorium-ligand bonds generally more labile than their U(IV) counterparts.<sup>13</sup> Since the seminal report by Liddle *et al.* on a binuclear Th complex bridged by two  $\mu_2$ –

alkoxide centers, there has been growing interest in actinide binuclear complexes.<sup>34</sup> The dithorium(IV)-phosphinidiide  $[(\text{Th}(\text{Tren}^{\text{TIPS}}))_2(\mu\text{-PH})]$  and dithorium(IV)- $\mu$ -phosphido  $[(\text{Th}(\text{Tren}^{\text{TIPS}}))_2(\mu\text{-P})][\text{Na}(12\text{C}4)_2]$  complexes, featuring Th–PH–Th and Th=P=Th linkages were successfully isolated, respectively.<sup>17,35</sup> Calculation results suggest that the 5f- and 6d-orbital components of  $[(\text{Th}(\text{Tren}^{\text{TIPS}}))_2(\mu\text{-PH})]$  and  $[(\text{Th}(\text{Tren}^{\text{TIPS}}))_2(\mu\text{-P})]$  are reasonably balanced at  $\sim 36$  and 50%, respectively, where thorium bonding is traditionally considered to have dominant 6d-orbital character whereas uranium is usually considered to have dominant 5f-orbital contributions.<sup>36</sup> Subsequently, analogous species  $[(\text{Th}(\text{Tren}^{\text{TIPS}}))_2(\mu\text{-AsH})]$  and  $[(\text{Th}(\text{Tren}^{\text{TIPS}}))_2(\mu\text{-As})][\text{K}(15\text{C}5)_2]$  with Th–AsH–Th and Th=As=Th units,<sup>18</sup> respectively, were also successfully isolated using a similar synthetic approach. The Th–As bonds in both complexes have obvious ionic properties. Meanwhile, the Th–N<sub>amide</sub> bonds in two ThN(H)Th complexes also showed obvious ionic characteristics.<sup>22</sup> These findings provide experimental evidence for constructing binuclear thorium complexes with a Th–X–Th unit.

Here, we report the synthesis and characterization of a binuclear thorium complex **3**,  $[(\text{Trapen}^{\text{TMS}}\text{Th})_2(\mu\text{-O})]$ , which contains a linear Th–O–Th core *via* *in situ* reduction. To elucidate the bonding nature of the Th–O–Th unit, we performed computational studies on these molecules using density functional theory (DFT) and localized bond orbital (LBO) methods. Compared with the Th–X–Th complexes reported by Liddle *et al.*,<sup>17,18</sup> this work not only expands the diversity of the Th–X–Th structural system, extending it from N and P to O, but also reveals that the Th–O bond exhibits greater covalent character than the Th–N bond. This finding challenges the conventional view that Th–O single bond is predominantly ionic.

## 2 Results and discussion

### 2.1 Synthesis

After stirring a tetrahydrofuran solution of  $\text{Trapen}^{\text{TMS}}\text{Li}_3$  with  $\text{ThCl}_4(\text{DME})_2$  from  $-30$  °C to room temperature for 12 h,<sup>37</sup> the

<sup>a</sup>State Key Laboratory of High-efficiency Utilization of Coal and Green Chemical Engineering, College of Chemistry and Chemical Engineering, Ningxia University, Yinchuan 750021, China. E-mail: xiangyuli432@126.com; gy202054@163.com

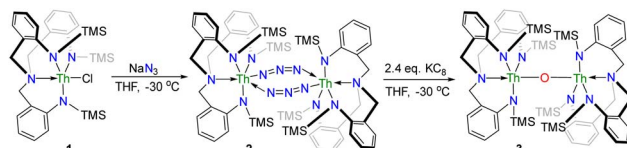
<sup>b</sup>Laboratory of Nuclear Energy Chemistry, Institute of High Energy Physics, Chinese Academy of Sciences, Beijing 100049, China. E-mail: yujipan@ihep.ac.cn

<sup>c</sup>Institute of Nuclear Fuel Cycle and Materials, School of Mechanical Engineering, Shanghai Jiao Tong University, Shanghai 200240, China. E-mail: shiwq@sjtu.edu.cn

<sup>d</sup>School of Science, China University of Geosciences, Beijing 100083, China

<sup>†</sup>These authors contributed equally to this manuscript.



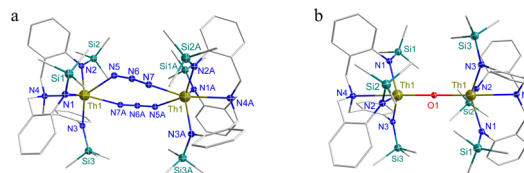


Scheme 1 Synthesis of complexes 1–3.

solvent was removed under vacuum. Then, the residue was extracted with toluene, and Trapen<sup>TMS</sup>ThCl(**1**) was obtained as a colorless solid in 70% yield (Scheme 1). The complex **2** was synthesized in moderate yield by adding a THF solution of **1** to a THF solution of Na<sub>3</sub>N (1.1 equiv) at -30 °C, along with elimination of NaCl. The structures of **1** and **2** were fully characterized by NMR and FT-IR spectroscopies. The <sup>1</sup>H NMR spectrum of **1** recorded in C<sub>6</sub>D<sub>6</sub> spans the range 0 to +8 ppm, which is consistent with the result that we previously reported.<sup>37,38</sup> For **2**, the <sup>1</sup>H NMR spectrum shows the range from 0 ppm to 7.18 ppm, similar to that of complex **1**. In addition, the FT-IR spectrum of **2** exhibits a strong azide stretching band at 2127 cm<sup>-1</sup> and 2086 cm<sup>-1</sup>, which is the characteristic of bridged thorium–azide bond.<sup>39</sup> The <sup>29</sup>Si NMR spectrum of complex **2** shows a rather remarkable signal with a single peak at -5.23 ppm. The reduction of complex **2** with 2.4 equivalent of KC<sub>8</sub> in THF caused the formation of complex **3**, which precipitated from toluene solution at -30 °C as colorless crystals in 42% yield. Complex **3** was fully characterized by means of spectroscopy and X-ray crystallography. The <sup>1</sup>H NMR spectrum indicates that the **3** exhibits C<sub>3</sub> symmetry, and resonance signals from 0 to +8 ppm assigned to 90 protons integrate properly. The TMS groups on the arylamine pendant arm were observed at 0.14 ppm. Unfortunately, no discernible signals were observed in the <sup>29</sup>Si NMR spectrum of complex **3**.<sup>41</sup>

## 2.2 Solid state structures

Owing to the inherent twinning and structural disorder in the crystal of complex **2**, multiple restraints were necessitated during the X-ray diffraction refinement process to stabilize the structural model. Given the uncertainties introduced by these refinement constraints, detailed discussion of bond lengths and angles for complex **2** is omitted herein. The solid-state molecular structures of **3** was confirmed by single crystal X-ray diffraction (Fig. 1). Complex **3** crystallizes in monoclinic space group P2<sub>1</sub>/c and the solid-state structure is shown in Fig. 1. The single-crystal X-ray analysis of **3** reveals a linear Th–O–Th (180.0(15)°) unit, which is an oxo-bridged binuclear structure. The Th–O distance is 2.271(2) Å, which is consistent with the sum of the covalent bond radii of thorium and oxygen (2.15 Å).<sup>40–43</sup> In addition, the Th–O bond lengths (2.271(2) Å) lie between the Th–OCP single bond length (2.331 Å) and the Th–OTMS single bond length (2.173 Å).<sup>26,38</sup> The ligand type and coordination mode significantly influence the bond lengths. Despite variations in bond distances, theoretical calculations reveal that the Th–O bond exhibits appreciable covalent character. The average distance Th–N<sub>amide</sub> is 2.333 Å and Th–N<sub>amine</sub> distance of complex **3** is (2.801(3) Å).

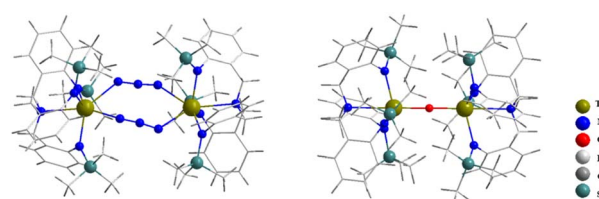
Fig. 1 Molecular structures of **2** (a), and **3** (b) from X-ray crystallography with 30% probability ellipsoids. Carbon atoms were represented in stick form. Hydrogen atoms were omitted for clarity.

## 2.3 Computational results

To explore the electronic structures and chemical bonding of complexes **2** and **3**, we performed quantum calculations and analyses using the Gaussian 16 program package<sup>44</sup> and Multifn 3.8 software<sup>45,46</sup> to investigate the structures and bonding nature of these complexes. Detailed computational methods are provided in the SI. The optimized structures are shown in Fig. 2. As shown in Table S3, the differences between gas-phase optimized structures (BP86/RECP/6-31G(d) theoretical level) and experimental crystal structures in terms of bond lengths are less than 0.1 Å. This indicates that the computational method is reliable for the studied complexes.<sup>47</sup> As a generalized gradient approximation (GGA) functional, BP86 has been widely used in computational studies of various complexes. Previous studies have confirmed its reliability in handling actinide complexes.<sup>38,47–51</sup> In this work, the structures optimized using BP86 were compared with the single-crystal structures of the studied complexes. The results show a good agreement between the structural parameters of the optimized complexes and the experimental data with bond length differences within 0.1 Å, indicating that BP86 is applicable to the studied complexes.

Previous studies have shown that for high-valent actinide complexes, spin-orbit coupling (SOC) has little effect on geometric structures.<sup>52</sup> Previously reported Th(IV) organometallic complexes (such as Th–Sb complexes) also did not include SOC effects in the corresponding calculations.<sup>20</sup> In addition, it has been shown that the results obtained using pseudopotential method for actinide complexes are generally consistent with those from all-electron calculations.<sup>53</sup> Therefore, for the studied closed-shell Th(IV) complexes, scalar relativistic effects were considered by the pseudopotentials without SOC effects in the calculations.

The covalency of the chemical bonds can be estimated by the bond order and localized molecular orbital (LMO) analyses.<sup>54</sup> The Wiberg bond indices (WBIs) of Th–N and Th–O bonds for complexes **2** and **3** are shown in Tables S5–S10. The WBIs values of Th–O bonds are significantly larger than Th–N bonds, showing the

Fig. 2 Optimized structures of complexes **2** and **3** at the BP86/RECP/6-31G(d) level of theory.

stronger covalent interactions of Th–O bonds. Meanwhile, the Th–N values decrease from 1.339 to 1.281 from complexes 2 to 3, which agrees with the trend of changes in bond lengths. For complex 3, the WBI value for the Th–O bond is relatively large (1.580). Since the WBI values are sensitive to the choice of computational methods,<sup>55</sup> to comprehensively evaluate the bonding characteristics of the Th–N and Th–O bonds, we performed calculations of WBIs and Mayer bond orders (MBOs) using different computational software programs and theoretical methods (B3LYP and BP86).<sup>56,57</sup> The results are presented in Tables S7–S12. As shown in Tables S7–S12, the trends in the MBO values of the Th–N and Th–O bonds are consistent with those of the corresponding WBI values, further supporting our conclusions.<sup>58</sup> Compared to the computed Th–O bond WBIs of the reported  $\text{Th}(\text{Tren}^{\text{TIPS}})\text{Cl}$  complex with thorium–oxygen linkages,<sup>26</sup> the calculated WBIs for complex 3 is 0.714 at the same theoretical level (B3LYP/ECP60MWB/6-31G(d)), significantly higher than reported WBIs (0.488). This confirms that the Th–O bond in the studied complex shows higher covalent character. Therefore, compared to the reported thorium bonding modes, the linear Th–O–Th mode exhibits stronger covalent interactions.

LMO analysis was also carried out for complexes 2 and 3 (Fig. S18, S19 and Table S11). As shown in Fig. S18 and Table S11, the  $\sigma$ -bonding orbitals are formed between the Th atoms and the N atoms of the ligands as well as the azide bonds ( $\text{N}=\text{N}=\text{N}$ ), while both  $\sigma$ - and  $\pi$ -bonding orbitals exist between the Th atom and O atoms.<sup>59</sup> The Th–N  $\sigma$ -bonding orbitals are mainly composed of contributions from the 7s and 6d orbitals of Th atoms and the 2s/2p orbitals of N atoms. The Th–O  $\sigma$ -bonding orbitals primarily involve the 7s, 6d, and 5f orbitals of Th and the 2p orbitals of O, whereas the  $\pi$ -bonding orbitals are formed through interactions between the 6d orbitals of Th and the 2p orbitals of O.

### 3 Conclusions

In summary, we obtained a binuclear thorium complex featuring a Th–O–Th unit through the *in situ* reduction, which was stabilized by a tripodal Trapen ligand. Density functional theory (DFT) results show that the Th–O bonding in complex 3 displays stronger covalent interactions. This work provides valuable insights to study the structure and bonding properties of binuclear complexes with Th–X–Th. In the future, we plan to explore potential applications in small molecule activation and catalysis.

## 4 Experimental

### 4.1 Caution!

As reactants, thorium-containing complexes exhibit both radioactivity and chemical toxicity. The handling of these substances in the experiment mandates strict adherence to safety protocols involving proper care and protection.<sup>32</sup>

### 4.2 General methods

All reactions were performed under an inert atmosphere of dry argon, employing either standard Schlenk techniques or a Vigor argon-filled glovebox, unless specified otherwise. The internal

oxygen and moisture levels in the glovebox atmosphere were monitored by an  $\text{O}_2/\text{H}_2\text{O}$  Analyzer to ensure both were less than 1 ppm.<sup>32</sup> The commercial reagents and solvents utilized in this study were procured from sources including J&K, Energy Chemical, Acros Organics, and other vendors. Solvents underwent drying and degassing *via* a Vigor solvent purification system. They were subsequently stored in Schlenk bottles, either above a sodium mirror under an argon atmosphere or over activated 4 Å molecular sieves (for THF). Drying of benzene-d<sub>6</sub> was performed over Na/K alloy, followed by storage under an argon atmosphere until use. All NMR spectra were performed using a Bruker AVACNEIII HD 500 spectrometers (<sup>1</sup>H 500 MHz) <sup>1</sup>H NMR chemical shifts ( $\delta$ ) were relative to tetramethylsilane (TMS) at room temperature.<sup>32</sup> Multiplicities are abbreviated as follows: singlet(s); doublet(d); triplet(t); quartet(q); multiplet(m); broad(br). Absolute values of the coupling constants, J, are provided in Hertz (Hz).<sup>32</sup> Crystals of all complex were examined using a Bruker D8 VENTURE X-ray CMOS diffractometer with a mirror-monochromated Mo  $\text{K}\alpha$  X-ray source ( $\lambda = 0.71073 \text{ \AA}$ ) or a Cu  $\text{K}\alpha$  X-ray source ( $\lambda = 1.54184 \text{ \AA}$ ) at 170 K.<sup>32</sup> Using Olex2, the structure was solved with the ShelXT structure solution program using Intrinsic Phasing. All non-hydrogen atoms were refined anisotropically. Hydrogen atoms were refined with constrained geometries and riding thermal parameters. All FT-IR spectra were recorded using a Bruker Tensor 27 with a KBr pellet.<sup>32</sup>

## Author contributions

The first three authors contributed equally to this work.

## Conflicts of interest

The authors declare no competing financial interest.

## Data availability

All other relevant data generated and analysed during this study, which include experimental, spectroscopic (NMR, IR, UV-Vis, CV), crystallographic and computational data, are included in this article and its supplementary information (SI). Supplementary information is available. See DOI: <https://doi.org/10.1039/d5ra09492e>.

CCDC 2468529 (3) contains the supplementary crystallographic data for this paper.<sup>60</sup>

## Acknowledgements

This work was financially supported by the National Natural Science Foundation of China (No. 22176191, 22266026, 22406098 and 22406186), the China Postdoctoral Science Foundation (No. 2024T170927), the Beijing Natural Science Foundation (No. 2232033), the Natural Science Foundation of Ningxia Province (2023AAC03014).



## References

- Y. Li, X. Xin, Q. Zhu and C. Zhu, *JACS Au*, 2024, **4**, 4612–4627.
- G. Zi, *Chem. Commun.*, 2018, **54**, 7412–7430.
- M. Keener, L. Maria and M. Mazzanti, *Chem. Sci.*, 2023, **14**, 6493–6521.
- G. I. Vargas-Zúñiga, M. A. Boreen, D. N. Mangel, J. Arnold and J. L. Sessler, *Chem. Soc. Rev.*, 2022, **51**, 3735–3758.
- J. T. Boronski, J. A. Seed, D. Hunger, A. W. Woodward, J. van Slageren, A. J. Woole, L. S. Natrajan, N. Kaltsoyannis and S. T. Liddle, *Nature*, 2021, **598**, 72–75.
- E. Lu, S. Sajjad, V. E. J. Berryman, A. J. Woole, N. Kaltsoyannis and S. T. Liddle, *Nat. Commun.*, 2019, **10**, 634.
- K. Liu, Y. Guo, J. Yu and W. Shi, *Acta Chim. Sin.*, 2023, **81**, 264–274.
- Z. Badri and C. Foroutan-Nejad, *Nat. Rev. Chem.*, 2024, **8**, 551–560.
- L. S. Natrajan, A. N. Swinburne, M. B. Andrews, S. Randall and S. L. Heath, *Coord. Chem. Rev.*, 2014, **266–267**, 171–193.
- O. Walter, *Chem.-Eur. J.*, 2019, **25**, 2927–2934.
- S. T. Liddle, *Angew. Chem., Int. Ed.*, 2015, **54**, 8604–8641.
- E. J. Schelter, R. Wu, B. L. Scott, J. D. Thompson, D. E. Morris and J. L. Kiplinger, *Angew. Chem., Int. Ed.*, 2008, **47**, 2993–2996.
- B. M. Gardner, P. A. Cleaves, C. E. Kefalidis, J. Fang, L. Maron, W. Lewis, A. J. Blake and S. T. Liddle, *Chem. Sci.*, 2014, **5**, 2489–2497.
- J. Du, G. Balázs, A. J. Woole, M. Scheer and S. T. Liddle, *Angew. Chem., Int. Ed.*, 2021, **60**, 1197–1202.
- Y. Zhang, M. Bhadbhade, L. Kong, I. Karatchevtseva and R. Zheng, *Polyhedron*, 2017, **138**, 82–87.
- Z. Zhao, K. Liu, Y. Guo, J. Yu and W. Shi, *Acta Chim. Sin.*, 2023, **81**, 1633–1641.
- E. P. Wildman, G. Balázs, A. J. Woole, M. Scheer and S. T. Liddle, *Nat. Commun.*, 2016, **7**, 12884.
- E. P. Wildman, G. Balázs, A. J. Woole, M. Scheer and S. T. Liddle, *Nat. Commun.*, 2017, **8**, 14769.
- T. M. Rookes, B. M. Gardner, G. Balázs, M. Gregson, F. Tuna, A. J. Woole, M. Scheer and S. T. Liddle, *Angew. Chem., Int. Ed.*, 2017, **56**, 10495–10500.
- J. Du, K. Dollberg, J. A. Seed, A. J. Woole, C. von Hänisch and S. T. Liddle, *Nat. Chem.*, 2024, **16**, 780–790.
- D. M. King, B. E. Atkinson, L. Chatelain, M. Gregson, J. A. Seed, A. J. Woole, N. Kaltsoyannis and S. T. Liddle, *Dalton Trans.*, 2022, **51**, 8855–8864.
- J. Du, D. M. King, L. Chatelain, E. Lu, F. Tuna, E. J. L. McInnes, A. J. Woole, L. Maron and S. T. Liddle, *Chem. Sci.*, 2019, **10**, 3738–3745.
- J. Du, K. Dollberg, J. A. Seed, F. Tuna, A. J. Woole, C. von Hänisch and S. T. Liddle, *J. Am. Chem. Soc.*, 2025, **147**, 4430–4437.
- M. Falcone, L. Barluzzi, J. Andrez, F. Fadaei Tirani, I. Zivkovic, A. Fabrizio, C. Corminboeuf, K. Severin and M. Mazzanti, *Nat. Chem.*, 2019, **11**, 154–160.
- X. Sun, X. Gong, Z. Xie and C. Zhu, *Chin. J. Chem.*, 2022, **40**, 2047–2053.
- J. Yu, K. Liu, Q. Wu, B. Li, X. Kong, K. Hu, L. Mei, L. Yuan, Z. Chai and W. Shi, *Chin. J. Chem.*, 2021, **39**, 2125–2131.
- K. Liu, Y. Guo, J. Zhao, J. Li, K. Hu, L. Mei, C. Xu, M. Tong, J. Yu, J. Li and W. Shi, *Angew. Chem., Int. Ed.*, 2025, **64**, e202516858.
- B. M. Gardner and S. T. Liddle, *Chem. Commun.*, 2015, **51**, 10589–10607.
- J. Du, D. Hunger, J. A. Seed, J. D. Cryer, D. M. King, A. J. Woole, J. van Slageren and S. T. Liddle, *J. Am. Chem. Soc.*, 2021, **143**, 5343–5348.
- W. Fang, I. Douair, A. Hauser, K. Li, Y. Zhao, W. Roesky Peter, S. Wang, L. Maron and C. Zhu, *CCS Chem.*, 2021, **4**, 2630–2638.
- Y. Guo, X. Li, K. Liu, K. Hu, L. Mei, Z. Chai, J. K. Gibson, J. Yu and W. Shi, *Inorg. Chem.*, 2023, **62**, 10684–10693.
- P. Wang, Y. Zhao and C. Zhu, *Organometallics*, 2022, **41**, 2448–2454.
- K. Liu, J.-P. Yu, Q.-Y. Wu, X.-B. Tao, X.-H. Kong, L. Mei, K.-Q. Hu, L.-Y. Yuan, Z.-F. Chai and W.-Q. Shi, *Organometallics*, 2020, **39**, 4069–4077.
- R. Shannon, *Acta Cryst. A*, 1976, **32**, 751–767.
- B. M. Gardner, W. Lewis, A. J. Blake and S. T. Liddle, *Organometallics*, 2015, **34**, 2386–2394.
- J. Du, J. Hurd, J. A. Seed, G. Balázs, M. Scheer, R. W. Adams, D. Lee and S. T. Liddle, *J. Am. Chem. Soc.*, 2023, **145**, 21766–21784.
- B. E. Bursten, L. F. Rhodes and R. J. Strittmatter, *J. Am. Chem. Soc.*, 1989, **111**, 2756–2758.
- K. Liu, X.-W. Chi, Y. Guo, Q.-Y. Wu, K.-Q. Hu, L. Mei, Z.-F. Chai, J.-P. Yu and W.-Q. Shi, *Inorg. Chem.*, 2022, **61**, 17993–18001.
- K. Liu, X. Chi, Y. Guo, K. Hu, L. Mei, J. Yu and W. Shi, *New J. Chem.*, 2024, **48**, 18241–18248.
- F.-C. Hsueh, L. Barluzzi, M. Keener, T. Rajeshkumar, L. Maron, R. Scopelliti and M. Mazzanti, *J. Am. Chem. Soc.*, 2022, **144**, 3222–3232.
- C. J. Windorff and W. J. Evans, *Organometallics*, 2014, **33**, 3786–3791.
- J. Du, C. Alvarez-Lamsfus, E. P. Wildman, A. J. Woole, L. Maron and S. T. Liddle, *Nat. Commun.*, 2019, **10**, 4203.
- B. Cordero, V. Gómez, A. E. Platero-Prats, M. Revés, J. Echeverría, E. Cremades, F. Barragán and S. Alvarez, *Dalton Trans.*, 2008, 2832–2838.
- P. Pykkö, *J. Phys. Chem. A*, 2015, **119**, 2326–2337.
- P. Pykkö and M. Atsumi, *Chem.-Eur. J.*, 2009, **15**, 186–197.
- M. J. Frisch, G. W. Trucks, H. B. Schlegel, G. E. Scuseria, M. A. Robb, J. R. Cheeseman, G. Scalmani, V. Barone, G. A. Petersson, H. Nakatsuji, X. Li, M. Caricato, A. V. Marenich, J. Bloino, B. G. Janesko, R. Gomperts, B. Mennucci, H. P. Hratchian, J. V. Ortiz, A. F. Izmaylov, J. L. Sonnenberg, Williams, F. Ding, F. Lipparini, F. Egidi, J. Goings, B. Peng, A. Petrone, T. Henderson, D. Ranasinghe, V. G. Zakrzewski, J. Gao, N. Rega, G. Zheng, W. Liang, M. Hada, M. Ehara, K. Toyota, R. Fukuda, J. Hasegawa, M. Ishida, T. Nakajima, Y. Honda,



O. Kitao, H. Nakai, T. Vreven, K. Throssell, J. A. Montgomery Jr, J. E. Peralta, F. Ogliaro, M. J. Bearpark, J. J. Heyd, E. N. Brothers, K. N. Kudin, V. N. Staroverov, T. A. Keith, R. Kobayashi, J. Normand, K. Raghavachari, A. P. Rendell, J. C. Burant, S. S. Iyengar, J. Tomasi, M. Cossi, J. M. Millam, M. Klene, C. Adamo, R. Cammi, J. W. Ochterski, R. L. Martin, K. Morokuma, O. Farkas, J. B. Foresman and D. J. Fox, *Gaussian 16*; Gaussian, Inc., Wallingford, CT, 2016.

47 T. Lu and F. Chen, *J. Comput. Chem.*, 2012, **33**, 580–592.

48 T. Lu, *J. Chem. Phys.*, 2024, **161**, 082503.

49 X. Chi, Q. Wu, C. Wang, J. Yu, K. Liu, R. Chi, Z. Chai and W. Shi, *Organometallics*, 2022, **41**, 1304–1313.

50 X. Chi, Q. Wu, C. Wang, J. Lan, R. Chi and W. Shi, *J. Mol. Struct.*, 2025, **1330**, 141519.

51 D. H. T. Amador, J. R. Sambrano, R. Gargano and L. G. M. de Macedo, *J. Mol. Model.*, 2017, **23**, 100.

52 L. Li, T. Stüker, L. Andrews, H. Beckers and S. Riedel, *Chem.–Eur. J.*, 2019, **25**, 1795–1805.

53 X. Cao, S. Lekat and M. Dolg, *J. Phys. Chem. Lett.*, 2025, **16**, 8216–8226.

54 S. Wei, H. Hu, W. H. E. Schwarz and J. Li, *Chem. Sci.*, 2025, **16**, 6744–6754.

55 *Experimental and Theoretical Approaches to Actinide Chemistry*, 2018, pp. , pp. 490–504.

56 R. F. W. Bader, *Chem. Rev.*, 1991, **91**, 893–928.

57 M. Michalski, A. J. Gordon and S. Berski, *Struct. Chem.*, 2019, **30**, 2181–2189.

58 I. Mayer, *Chem. Phys. Lett.*, 1983, **97**, 270–274.

59 A. E. Reed, R. B. Weinstock and F. Weinhold, *J. Chem. Phys.*, 1985, **83**, 735–746.

60 CCDC 2468529: Experimental Crystal Structure Determination, 2025, DOI: [10.5517/ccdc.csd.cc2nvpz6](https://doi.org/10.5517/ccdc.csd.cc2nvpz6).

